JBC Papers in Press. Published on June 13, 2018 as Manuscript RA118.003557
The latest version is at http://www.jbc.org/cgi/doi/10.1074/jbc.RA118.003557

Directed evolution of a picomolar affinity, high-specificity antibody targeting phosphorylated tau

Dan Li[1], Lei Wang[2], Brandon F. Maziuk[3], Xudong Yao[2, 4], Benjamin Wolozin[3], Yong Ku Cho[1, 4, 6]*

[1]Department of Biomedical Engineering, [2]Department of Chemistry, University of Connecticut, Storrs CT 06269; [3]Boston University School of Medicine, Department of Pharmacology and Experimental Therapeutics, Boston, MA 02118; and [4]Institute for Systems Genomics, [5]Department of Chemical and Biomolecular Engineering, University of Connecticut, Storrs CT 06269, United States

Running title: *High Affinity and Specificity Phospho-Tau Antibody*

*To whom correspondence should be addressed: Yong Ku Cho: Departments of Chemical and Biomolecular Engineering and Biomedical Engineering, Institute for Systems Genomics, University of Connecticut, Storrs CT 06269; cho@uconn.edu; Tel. (860) 486-4072; Fax. (860) 486-2959.

Keywords: Neurodegeneration, antibody, Tau protein, protein phosphorylation, immunochemistry, phospho-specific, affinity, antibody specificity, post-translational modification, anti-PTM antibody, scFv

ABSTRACT

Antibodies are essential biochemical reagents for detecting protein post-translational modifications (PTMs) in complex samples. However, recent efforts in developing PTM-targeting antibodies have reported frequent non-specific binding and limited affinity of such antibodies. To address these challenges, we investigated whether directed evolution could be applied to improve the affinity of a high-specificity antibody targeting phospho-threonine 231 (pT231) of the human microtubule-associated protein tau. On the basis of existing structural information, we hypothesized that improving antibody affinity may come at the cost of loss in specificity. To test this hypothesis, we developed a novel approach using yeast surface display to quantify the specificity of PTM-targeting antibodies. When we affinity-matured the single-chain variable antibody fragment through directed evolution, we found that its affinity can be improved > 20-fold over that of the wild-type antibody, reaching a picomolar range. We also discovered that most of the high-affinity variants exhibit cross-reactivity towards the non-phosphorylated target site, but not to the phosphorylation site with a scrambled sequence. However, systematic quantification of the specificity revealed that such a tradeoff between the affinity and specificity did not apply to all variants and led to the identification of a picomolar-affinity variant that has a matching high specificity of the original phospho-tau antibody. In cell- and tissue-imaging experiments, the high-affinity variant gave significantly improved signal intensity while having no detectable nonspecific binding. These results demonstrate that directed evolution is a viable approach for obtaining high-affinity PTM-specific antibodies, and highlight the importance of assessing the specificity in the antibody engineering process.

INTRODUCTION

Antibodies that target post-translationally modified proteins are widely used in biology and clinical investigations. Some antibodies can bind to a single modified amino acid (e.g., phosphorylated tyrosine) within the context of diverse nearby peptide sequences (1,2). However, most widely used are antibodies specific to a modification site in a defined target protein sequence, herein referred to as post-translational modification (PTM)-specific antibodies. Due to a large number of experimentally identified post-translational modification sites (> 87,000) (3), the demand for PTM-specific antibodies continues to grow.

PTM is a key mechanism that enables reversible regulation of protein activity, conformation, localization, turnover rate, and interactions. Abnormal PTMs result in dysregulation of these processes and are often associated with pathological conditions. In case of the microtubule-associated protein tau, numerous abnormal PTMs regulate its biology, and are associated with several neurodegenerative diseases including Alzheimer's disease (AD), collectively referred to as tauopathies (4). Tau contains 85

putative phosphorylation sites (5) and 14 putative acetylation sites (6). Phosphorylation sites at or near the repeat elements of the microtubule binding domains are particularly important for the pathophysiology of tauopathy (7). An increase in tau phosphorylation, on average from 2-3 to 7-8 phosphate per molecule (7) results in preferential phosphorylation at sites that decrease microtubule binding (8,9), and increases its propensity to form oligomers and high order aggregates (7,10). Levels of tau oligomers showed a strong correlation with memory loss in a mouse model of tauopathy (11). Acetylation at specific lysine residues interferes with ubiquitination and subsequent degradation by the proteasome, resulting in accumulation of phosphorylated tau and associated toxicity in mouse models (12-15). Therefore, detection of tau PTMs at specific sites is valuable in identifying the cause and tracking the progression of tauopathies.

However, robust detection of PTMs is challenging due to their dynamic and heterogeneous nature. Only a fraction of a protein is modified at any given time, and the dynamics may vary within a tissue across different cell types (16-18). Therefore, the affinity and specificity of PTM-specific antibodies are critical for sensitive and reproducible detection of PTMs (19). PTM-specific antibodies should interact only with the modified target site, with high affinity to capture potentially a small fraction of the modified form. In case of tau PTM-specific antibodies, their affinity and specificity are particularly important, since they dictate their efficacy in a wide range of applications. High-affinity antibodies are superior in detecting tau PTMs from clinical samples (20), but mouse model experiments suggest that high specificity antibodies may be more beneficial for passive immunotherapy targeting tau (21).

Even though many PTM-specific antibodies exist, high-affinity antibodies with high PTM-specificity are rarely found. Rodent immunization approaches often fail or produce low-affinity antibodies. This is because the peptide epitopes containing PTMs are weak immunogens in mice (22), PTMs undergo rapid degradation *in vivo* regardless of the immunization route (23), and B-cell response shows an affinity ceiling (24,25). Screening recombinant antibody libraries *in vitro* is a promising alternative. However, *in vitro* library screening strategies tend to generate PTM-specific antibodies with a low or moderate affinity (K_d ~ μM to 100 nM range) (26-29).

Obtaining high specificity antibodies targeting PTMs is even more challenging. In fact, many commercially available PTM-specific antibodies have not been validated for their specificity. Recent evidences using various approaches, including immunoassays using synthetic peptides and peptide arrays, have shown that indeed a significant fraction of existing PTM-targeting antibodies lack specificity (30-34). These studies have identified major species that non-specifically bind to the antibodies, including non-modified epitopes with the target amino acid sequence and those with modifications at non-target sites (31,34).

Recently, X-ray crystal structures of phospho-specific antibodies have revealed a key insight on how PTM-targeting antibodies may gain specificity (26,27). In these antibodies, a set of complementarity determining region (CDR) residues were found to interact with the phosphate group, while others make contacts with the amino acid residues nearby, leading to recognition of both the modification and target sequence. Therefore, balancing the stability of interaction of these distinct sets of CDR residues seems to be important in gaining both the affinity and specificity. It is plausible that high-affinity PTM-targeting antibodies can achieve such tight binding by stabilizing the interaction towards either the modified amino acid or peptide sequence, potentially leading to unwanted cross-reactivity. Therefore, we hypothesized that a trade-off between affinity and specificity might exist in PTM-targeting antibodies.

To test this hypothesis, we sought to assess the impact of *in vitro* affinity maturation on the specificity of PTM-targeting antibodies. Starting from an existing high-specificity antibody (27) targeting phosphorylated T231 of human tau (pT231, numbering based on the 441 amino acid 2N4R isoform), we generated a single-chain variable fragment (scFv) and improved its affinity using directed evolution. To assess the specificity of PTM-targeting antibodies, we developed an experimental approach based on yeast surface display (35) to quantify scFv binding against a defined set of structurally similar epitopes. Specifically, peptides representing the phosphorylated epitope, non-phosphorylated

epitope, or a phosphorylated epitope with the same amino acid composition, but scrambled sequence were labeled for detection. Their interactions with yeast displayed antibody fragments were quantified using flow cytometry. Indeed, the original high-specificity phospho-tau scFv showed nearly perfect specificity in this assay, in agreement with previous characterizations (27). We found that through directed evolution, the affinity could be improved by > 20-fold, reaching picomolar monovalent dissociation constants. However, the majority of affinity-improved scFvs showed significant non-specific binding to the non-phosphorylated epitope but not to the scrambled phospho-epitope, suggesting that high-affinity clones tend to gain affinity by stabilizing the interaction with the amino acid residues surrounding the modification site. Even though the majority of clones showed a trade-off between their affinity and specificity, this was not necessarily the case for some unique clones. By assessing the binding specificity, we identified a picomolar-affinity clone with specificity profiles that match the original high-specificity antibody. These results demonstrated that a quantitative assessment of both affinity and specificity was critical for identifying high affinity and specificity antibodies targeting PTMs.

Results

Yeast surface display of a phospho-tau-specific scFv

To test our hypothesis, we first developed an assay to quantify antibody specificity using yeast surface display (**Fig. 1**). Synthetic peptides that represent the exact target epitope, as well as other potentially cross-reacting species were labeled for detection. Since yeast surface display allows surface expression of 40,000-50,000 single chain antibody fragments (scFvs) per cell (35,36), we anticipated that binding of multiple structurally-related epitopes displayed on yeast could be quantified using multicolor flow cytometry (**Fig. 1**). To demonstrate this concept, we used the previously identified high-specificity anti-phospho-tau antibody which targets pT231 (27). We cloned the antibody as a VL-VH single-chain variable region fragment (pT231 scFv), fused to the N-terminus of the yeast cell wall protein Aga2p (**Fig. 1**). To detect the interaction between pT231 scFv and the target phosphoepitope, a synthetic phosphopeptide (KKVAVVR(pT)PPK(pS)PSSAKC) was labeled with biotin at the C-terminal cysteine using maleimide-PEG_{11}-biotin. The resulting peptide was purified using high-performance liquid chromatography (HPLC), and the label was validated using mass spectrometry (**Supp. Fig. 1**). The scFv expression on the yeast cell surface and binding to the biotinylated phosphoepitope were confirmed using confocal microscopy (**Fig. 2*A***), using streptavidin-R-phycoerythrin (SA-PE) as a detection reagent. The affinity (dissociation constant K_d) of the yeast displayed pT231 scFv, as determined by titrating the biotinylated phosphopeptide (Pphos-b) was 2.2 ± 0.4 nM (**Fig. 2*B***, mean ± standard deviation), which is lower than the monovalent affinity for the full-length IgG (K_d = 0.35 nM) generated using the same variable regions (27). Even though scFv constructs are highly advantageous for imaging (37) and delivery (38-40), a 5 to 15-fold reduction in affinity upon conversion of IgG to scFv had been reported (38,41), potentially due to higher stability and functional concentration of full IgGs. To confirm that the yeast displayed scFv was properly folded, we generated alanine point mutations in the CDR residues that interacted with the phosphoepitope (**Supp. Fig. 2**), according to the published x-ray structure of the antibody-phosphopeptide complex (27). Alanine point mutations in all phosphoepitope interacting CDRs (single alanine substitutions in either CDR-H2, CDR-H3, CDR-L1, CDR-L2, or CDR-L3) substantially reduced phosphopeptide binding (**Supp. Fig. 2**), indicating that CDR residues were correctly presented in the yeast displaying scFv.

Assessment of antibody phospho-specificity using yeast surface display

Having verified the binding activity of the pT231 scFv, we quantified the specificity of the scFv to structurally similar epitopes, including the non-phosphoepitope and a phosphoepitope with scrambled amino acid sequence. We labeled peptides representing the non-phosphoepitope (Pnonphos, KKVAVVRTPPKSPSSAKC) and a scrambled phosphoepitope (Pscram, KAV(pS)ASVPVSRK(pT)KPPKC) with biotin at the C-terminal cysteine (**Supp. Fig. 1**, data not shown). To enable quantitation of binding specificity, we generated a phosphopeptide labeled with a second tag, Alexa 488, using Alexa Fluor

488 C_5 maleimide (**Supp. Fig. 1**). When we assessed the binding of pT231 to the phosphopeptide labeled with Alexa 488 (Pphos-A488) using flow cytometry, we found that the signal intensity of scFv-phosphopeptide was lower, compared to the signal obtained from Pphos-b (**Supp. Fig. 3**). Such a difference could be attributed to the fact that the brightness of R-phycoerythrin (molar absorption coefficient × quantum yield = 19.6×10^5 $M^{-1}cm^{-1} \times 0.82 = 16.1 \times 10^5$ $M^{-1}cm^{-1}$) (42) is 24-fold higher than that of Alexa 488 (0.73×10^5 $M^{-1}cm^{-1} \times 0.92 = 0.67 \times 10^5$ $M^{-1}cm^{-1}$, manufacturer specifications). Therefore, we amplified the signal from Alexa 488, using an anti-Alexa 488 antibody (rabbit polyclonal) followed by an anti-rabbit IgG conjugated with Alexa 488, which resulted in 10-fold increase in the scFv-Pphos-A488 signal (**Supp. Fig. 3**). When yeast cells displaying the pT231 scFv were incubated with an equimolar mixture of Pphos-b and Pphos-A488 (both at 0.5 μM), signals from both labels were detected using flow cytometry (**Fig. 2*C***), as anticipated in the multi-color labeling scheme (**Fig. 1**). To assess the specificity, yeast cells displaying pT231 scFv were incubated with a mixture of either Pphos-A488 and Pnonphos-b (both at 0.5 μM) or Pphos-A488 and Pscram-b (both at 0.5 μM). In these experiments, the yeast cells showed labeling almost exclusively by the target phosphopeptide (Pphos-A488), and no detectable binding to the non-phosphopeptide (Pnonphos-b) or scrambled phosphopeptide (Pscram-b) (**Fig. 2*C***). These results confirmed the previous report of high specificity of the pT231 antibody (27), and demonstrated the effectiveness of our specificity quantification assay.

Directed evolution of pT231 scFv for improved affinity

We performed directed evolution of the pT231 scFv by applying selection pressure to enhance the affinity (**Fig. 3a**). We generated a random mutation library of the pT231 scFv using error-prone PCR (43) followed by electroporation in yeast (44), yielding approximately 3×10^7 transformants displaying the scFv variants. The scFv library was subjected to three rounds of fluorescence-activated cell sorting (FACS) (**Fig. 3a**). After round 1 and 2, the sorted scFv sequences were further diversified using DNA shuffling followed by random mutagenesis (**Fig. 3a**). Throughout the FACS process, selection pressure for higher affinity was applied by incubating yeast cells displaying pT231 mutants with progressively lower concentration of Pphos-b (**Fig. 3a**) followed by incubation with 1 μM of unlabeled phosphopeptide (Pphos) for dissociation (45), and sorting for high Pphos-b binding vs. scFv expression (using anti-c-Myc antibody) (**Fig. 3b**). After three rounds of FACS, a population of high Pphos-b was enriched (**Fig. 3c).** We sequenced individual clones from this pool and identified 27 unique scFv mutant sequences (**Fig. 4**). Even though all 27 clones had distinct sequences with mutations throughout the scFv sequence, several high occurrence mutations were found (**Fig. 4**). The majority of frequent mutations (residues with occurrence labeled in bold in **Fig. 4**) were found in or near the CDRs (Kabat numbering): V_LW50L and V_LS56C (L2), V_LA95T, V_HG100$_H$D (or S), V_HD101G, and V_HA102T (H3) (**Fig. 5**). Mutations V_LD57G, V_HG74C, and V_HA93V were in the framework regions (**Fig. 5**).

Characterization of affinity and specificity of scFv mutants

To assess the effectiveness of the directed evolution, we characterized the clones isolated after three rounds of sorting for their affinity and specificity. For these analyses, we chose the first 14 unique clones identified from sequencing (clones 3.1 to 3.14, **Fig. 4**). To rapidly compare the affinity to that of the WT pT231 scFv, we incubated yeast cells displaying mutant scFvs with 2 nM of Pphos-b, which was near the K_d of the wild-type pT231 scFv. At this peptide concentration, 7 out of 14 clones showed significantly higher binding (normalized to the scFv expression level) compared to that of the WT scFv (**Fig. 6a**, $P < 0.05$, Dunnett's multiple comparisons test). Based on the binding/expression level, we chose scFv mutant 3.05 (containing 6 mutations, **Fig. 4**) and measured its affinity by displaying it on yeast and generating a titration curve for the Pphos-b binding (**Fig. 6b**). scFv 3.05 showed a 21-fold improvement in affinity over that of the WT pT231 scFv, reaching picomolar monovalent binding affinity ($K_d = 92 \pm 1$ pM) (**Fig. 6b**). To characterize the phospho-specificity of the 14 mutant clones, we first measured the individual binding to Pnonphos-b and Pscram-b of the 14 clones (**Fig. 6c, d**). We found

that of the 14 clones, 6 showed significant binding to the Pnonphos-b (**Fig. 6c**, $P < 0.01$, Dunnett's multiple comparisons test), while none of the clones showed detectable binding to the Pscram-b (**Fig. 6d**). When we assessed the specificity of the high-affinity scFv 3.05 using competitive binding between Pphos-A488 and Pnonphos-b, significant binding to Pnonphos-b was detected (**Supp. Fig. 4**). Taken together, these results suggested that some of the clones gained affinity by stabilizing the interaction to the target peptide sequence, while none of the clones gained affinity to the phosphate group alone to cause cross-reactivity towards Pscram-b. Conversely, the fact that some of the clones did not show significant binding to the Pnonphos-b (**Fig. 6c**) suggested that improving affinity did not necessarily lead to enhanced cross-reactivity towards the non-phosphorylated epitope. In order to identify an optimal clone with improved affinity and high specificity, we selected additional clones based on the sequence homology and occurrence of mutations (**Fig. 4**), and assessed their binding to Pphos-b, Pnonphos-b, and Pscram-b. From this characterization, we identified scFv 3.24 (containing 5 mutations) that showed 11-fold of improvement in binding affinity over the wild-type pT231 (**Fig. 6e**, K_d = 160 ± 50 pM) and no significant change in binding to Pnonphos-b compared to that of wild-type pT231 (**Fig. 6f**). These results indicate that in phospho-specific antibodies, applying selection pressure towards improved affinity does result in cross-reactivity in a significant fraction of clones. Therefore, high-affinity clones need to be checked for phospho-specificity in order to improve the binding affinity through directed evolution.

Cell and tissue section labeling using purified scFvs

High affinity and specificity reagents are expected to enable sensitive detection of tau phosphorylation in complex samples. We tested the performance of the scFvs in immunocytochemistry and immunohistochemistry experiments. In order to perform the labeling experiments, we cloned the wild-type scFv and mutant 3.24 into a vector containing a synthetic secretion signal (46) to secrete them using yeast *S. cerevisiae*. The secreted scFvs were purified using a hexa-histidine motif at the C-terminus (**Supp. Fig. 5**). When we resolved the purified scFvs using SDS-PAGE followed by Coomassie staining, the gel loaded with purified scFvs showed a single protein band with a molecular weight of 28 kDa, which is typical for scFvs (47), with ~92% purity as quantified by densitometry of the gel (**Supp. Fig. 5**). To enable direct imaging of the scFvs without the use of secondary reagents, the purified scFvs were fluorescently labeled with Alexa 594 through modification of lysine residues (NHS-Alexa Fluor 594) and purified. In order to assess the specificity, the fluorescent scFvs were used to label human embryonic kidney cells (HEK293FT) transiently expressing human tau (microtubule-associated protein tau (MAPT) 0N4R) as a GFP fusion (EGFP-tau) (48). When high concentrations (100 nM) of the wild-type pT231 scFv or scFv 3.24 were used for staining, clear scFv signal was detected in HEK293FT cells expressing wild-type tau (**Fig. 7a**, top row) but not to the same cells treated with λ phosphatase (**Fig. 7a**, second row). These results indicate that the binding of wild-type pT231 scFv and mutant 3.24 requires phosphorylation of tau, and as reported previously, the tau expressed in HEK293 cells is phosphorylated (49,50). In order to further assess the specificity of the scFvs, we generated point mutants of human tau at the target phosphorylation site (T231) either incapable of phosphorylation (T231A) or pseudophosphorylated (T231E). In HEK293FT cells expressing EGFP-tau T231A, both the wild-type pT231 scFv and mutant 3.24 showed no detectable binding (**Fig. 7a**, third row), while in the same cells expressing EGFP-tau T231E, both scFvs showed clear binding (**Fig. 7a**, bottom row). These results indicate that the scFv binding requires tau phosphorylation at T231. When we compared the labeling of wild-type and scFv 3.24 at lower concentrations, scFv 3.24 showed significantly higher binding signal above background compared to that of wild-type at scFv concentrations ranging from 80 pM to 50 nM (**Fig. 7b**, $P < 0.05$, student's t-test).

We proceeded to test the fluorescently labeled scFvs in the staining of tissue sections from both PS19 mouse tissue slices and human AD tissue slices; PS19 mice expressed the aggregation-prone mutant P301S of human tau (1N4R) under the mouse prion protein (*Prnp*) promoter (51). In brain slices of 8-month old PS19 mice, wild-type pT231 scFv and mutant 3.24 demonstrated staining patterns characteristic of neurofibrillary tangles (**Fig. 8a**), suggesting specific labeling of tau. This

staining was dose-dependent for both scFvs (**Fig. 8b**). Neither scFv showed detectable staining in either tau knock-out or wild type C57Bl/6 mice (**Fig. 8c**). Staining of human AD tissue also revealed characteristic tangle staining (**Fig. 8d**) with no detectable staining in aged control brain tissues. However, in the human tissues the mutant scFv 3.24 showed significantly higher signal than the wild-type scFv at the 50 nM working concentration (**Fig. 8e**), suggesting higher affinity and more robust staining for the mutant scFv. These results further demonstrate that the high-affinity antibody generated in this study has exceptionally high specificity for phospho-tau.

Discussion

In this study, we applied directed evolution to enhance the affinity of a phospho-specific antibody, and quantified the impact of *in vitro* affinity maturation on specificity. High-affinity antibody fragments with dissociation constants reaching picomolar range were successfully generated. Based on the crystal structure of the wild-type pT231 antibody bound to the phosphopeptide (27), only one mutation occurred in a residue that directly contacts the phosphoepitope (**Fig. 5**, V_LW50L). Five out of 9 high occurrence mutations were located near the direct contact sites (V_LS56C, V_LA95T, V_HG100$_H$D (or S), V_HD101G, and V_HA102T). The pattern of mutations occurring in amino acid positions near, but not at the direct contact site has been frequently observed in high affinity antibody variants (52,53). Such mutations may contribute to enhanced affinity through preorganization and rigidification of the paratope (54-56). Mutations V_HG100$_H$D, V_HD101G, and V_HA102T are also located at the VH-VL interface, suggesting that stability of interaction between the two domains may contribute to affinity improvement. Interestingly, high occurrence mutations found in the optimal variant 3.24 (V_LD57G, V_HG74C, and V_HA93V) were exclusively located in the framework region. This suggests that this variant may have gained affinity through optimization of structural plasticity (57,58). Further investigation on the impact of individual mutations on affinity and specificity may provide new insights on designing PTM-specific antibodies.

High-affinity reagents would be highly advantageous in detecting PTMs from complex samples. Our results show that the high affinity variant scFv generated significantly higher signal compared to that of the wild-type scFv in detecting tau from human tissue, but not in mouse tissue. The discrepancy in staining intensities may be explained by differences in the expression level of human tau and level of phosphorylation. In the transgenic mice PS19, the expression of human tau P301S is driven by the prion protein promoter, which is strongly induced in neuronal cells (59), leading to 3-5 fold higher levels of tau expression than endogenous levels (51). Moreover, in PS19 mice, the solubility of tau decreases by 3 months of age, and becomes hyperphosphorylated (51,60). Therefore, the level of insoluble aggregates of phosphorylated tau in the mouse tissue may be significantly higher than in human AD patient tissue. Additionally, in the mouse tissue, the labeling intensity was significantly diminished at a scFv concentration of 10 nM, suggesting a possibility for mass transfer limitation of the labeling reagent. Very slow or limited antibody penetration has been reported for fixed samples (61). This shows the need for high antibody concentrations in labeling fixed tissue, and highlights the importance of antibody specificity.

While the scFv identified in this study can be converted to full-length IgGs, the scFv construct provides unique advantages for detecting tau due to its small size. Compared to full-length IgGs (150 kD), scFvs are approximately one-sixth in molecular weight (25 kD). This has led to significant enhancement in processes that rely on diffusion, such as tissue penetration. For example, when the blood-brain barrier was transiently opened through focused ultrasound, scFvs showed 5- to 57-fold higher uptake into the central nervous system compared to IgGs (40). In a mouse model of tauopathy, intravenously injected scFvs were detected in the brain tissue in significantly higher levels compared to that of IgGs (37). Moreover, scFv constructs enable wider modes of delivery since they are encoded by a short single gene that can be packaged in viruses. For example, intracerebroventricular injection of adeno-associated viruses carrying an anti-tau scFv resulted in reduced tau accumulation in a mouse model of tauopathy (39). Finally, we demonstrated cell and tissue staining using scFvs directly labeled with a fluorophore. These reagents have the potential to enable sub-diffraction limit imaging of phospho-tau

due to greatly reduced linkage error, which limit image resolution (62).

Phosphorylation of tau at T231 is a widely recognized modification for its association with AD. *In vitro* and in cultured cells, pT231 decreases the ability of tau to bind and stabilize microtubules (63,64). pT231 seems to occur early in AD progression and precedes paired helical filament (PHF) formation (65). pT231 was found in the cerebrospinal fluid (CSF) of patients with mild cognitive impairments who eventually developed AD (66). In addition, levels of pT231 in the CSF were correlated with rates of hippocampal atrophy in AD patients (67). An immunoassay of pT231 in the CSF demonstrated a 85% sensitivity (detection in 23 out of 27 AD samples) and a 97% specificity (detection in 1 out of 31 non-AD samples) in AD brain extracts (68). The high affinity and specificity pT231 tau antibody developed in this study is expected to enhance the sensitivity and enable earlier detection of pT231.

A major finding of this study is that *in vitro* affinity maturation of the phospho-specific antibody led to an increase in unwanted cross-reactivity towards the non-phosphorylated target sequence in a majority of high-affinity variants. Considering the fact that the area of interaction available from a modified amino acid is limited, stabilization of interaction with the nearby amino acid sequence may be a common phenomenon in high-affinity PTM-specific antibodies. In a recent study, monoclonal antibodies generated in guinea pig against pT18 of p53 showed picomolar affinity (K_d = 0.20 nM) but also significant binding to the non-phosphorylated p53 (K_d = 130 nM) (69). If such antibody is used at concentration ranges commonly used for cell or tissue staining (10 - 50 nM), false positive signal from cross reactivity towards the non-modified target may be detected. This illustrates an important point that antibody specificity is a function of antibody concentration. Therefore, existing PTM-specific antibodies should be validated for their specificity under varying concentrations. We suggest setting an upper concentration limit for each PTM-specific antibody to prevent false positive detection. Until now, efforts to validate and enhance specificity has been rarely made. Non-specific antibodies would be a major factor in irreproducibility in biological experiments. Ongoing efforts to standardize ways to quantify and document specificity of binding reagents (70) need to consider these aspects of antibody specificity.

We introduced an approach using yeast surface display to quantify the specificity of PTM-targeting antibodies. This enabled us to find that even among antibody variants selected only for improved affinity, a fraction of clones maintained high specificity. This specificity quantification approach may be widely adopted due to the general applicability of yeast surface display and its compatibility with flow cytometry. We demonstrated the use of this approach for a phospho-specific antibody, but it is readily applicable to other PTM-specific antibodies. In principle, this approach would be suitable for assessing the specificity of affinity reagents in general. The identified high-affinity variant showed exceptional specificity, as validated by cell and tissue staining experiments. Due to the compatibility with FACS, this approach has potential to enable directed evolution of antibody specificity. In particular, it would be useful in engineering the specificity of antibodies with known cross-reactivity. For example, a recent study showed that a significant fraction of commercially available PTM-specific tau antibodies has cross reactivity (34). Directed evolution may be applied to reduce the cross-reactivity of these antibodies.

The results from this study demonstrate that *in vitro* affinity maturation is a viable option for improving the affinity of PTM-specific antibodies. In this process, it is essential to quantify the specificity, particularly to the non-modified target sequence. By quantifying the specificity, it is possible to apply selection pressures for improved affinity and specificity simultaneously.

Experimental procedures

Yeast surface display of pT231 scFv

Amino acid sequence of VL and VH from an anti-tau pT231 antibody (27) was back-translated to DNA sequence, yeast-codon optimized and synthesized (Integrated DNA Technologies). A $(G_4S)_3$ linker was inserted between the VL and VH sequences (5'-VL-linker-VH) to create a fusion construct encoding a scFv sequence. The synthesized scFv gene was cloned using polymerase chain reaction (PCR) to add a 5' *Nhe*I and a 3' *BsrG*I (New England Biolabs) restriction sites. The PCR products were ligated into the vector pCT4RE (35) (a gift from Dr. Eric

Shusta). This plasmid included an N-terminal c-myc epitope tag and a C-terminal FLAG epitope tag. The pCT4RE plasmid was transformed into *S. cerevisiae* EBY100 (35) (a gift from Dr. Dane Wittrup).

Peptide modification and purification

All peptides used were purchased from a commercial source (Peptide 2.0). Peptides contained a C-terminal cysteine for chemical modification. Peptides to be modified were dissolved at 1 mM in phosphate-buffered saline (PBS, 8 g/L NaCl, 0.2 g/L KCl, 1.44 g/L Na_2HPO_4, 0.24 g/L KH_2PO_4, pH 7.4) at room temperature. A 10 mM stock solution of Alexa Fluor 488 C_5 maleimide (Thermo Fisher Scientific) was prepared in deionized H_2O, and a 100 mM stock solution EZ-link maleimide-PEG_{11}-biotin (Thermo Fisher Scientific) was prepared in dimethyl sulfoxide (DMSO). The Alexa Fluor 488 C_5 maleimide stock solution was protected from light by wrapping container with aluminum foil. For peptide modification, either Alexa Fluor 488 C_5 maleimide or EZ-Link maleimide-PEG_{11}-biotin stock solution was added to the peptide PBS solution at a final reagent concentration of 2 mM. The reactions proceeded at 4 ^oC overnight in the dark.

Modified peptides were purified using an HPLC system (Shimadzu SCL-10Avp), equipped with a preparative column (Waters, Atlantis T3, 100 Å, 10 µm, 10 mm x 250 mm). For the mobile phase, solvent A consisted of 99.9 % H_2O and 0.1 % trifluoroacetic acid, and solvent B consisted of 99.9 % methanol and 0.1 % trifluoroacetic acid. Solvent flow rate was 3.5 mL/min. The column temperature was set at 50 ^oC. For each HPLC run, 100 µL of the peptide reaction mixture was injected. The gradient for peptides was as following: 0 % solvent B at 0 min, 20 % solvent B at 1 min, 40 % solvent B at 26 min, solvent 75 % B at 31 min, and 100 % solvent B at 36 min. Purified peptide fractions, which were detected at 214 nm, were collected, lyophilized, and stored at - 20 ^oC.

Mass spectrometry of the modified peptides was conducted using a QStar Elite hybrid QTOF mass spectrometer (AB Sciex). TOF spectra ((300-2000 *m/z*) were acquired using Analyst QS 2.0 software.

Directed evolution of the pT231 scFv

pT231 scFv was randomly mutagenized as described previously (71) with the following modifications. Error-prone PCR using a mixture of triphosphates of nucleoside analogs. Each PCR consisted of ~ 250 ng of plasmid template, 0.5 µM of forward and reverse primer, 200 uM of dNTP mix (Thermo Fisher Scientific), Taq PCR buffer (without $MgCl_2$), 2 mM of $MgCl_2$, 2.5 units of Platinum Taq DNA polymerase (Thermo Fisher Scientific), 2 µM of 8-Oxo-2'-deoxyguanosine-5'-triphosphate (Tri-Link Biotechnologies, 8-Oxo-dGTP) and 2 µM of 2'-Deoxy-P-nucleoside-5'-Triphosphate (Tri-Link, Biotechnologies dPTP) in a 50 µL of reaction volume. The mixture was denatured at 94 ^oC for 3 min followed by 19 cycles of 94 ^oC for 45 s, 55 ^oC for 30 s, and 72 ^oC for 60 s and a final extension of 72 ^oC for 10 min on a thermocycler. The PCR product was gel-purified using a gel extraction kit (Zymo Research). 2 µL of purified mutagenesis product was added to a 100 µL of PCR reaction solution without using nucleoside analogs to amplify the mutated fragments. About 6.4 µg of mutated pT231 scFv gene, and 1 µg of vector pCT4RE (a gift from Dr. Eric Shusta) were combined with 200 µL of electrocompetent EBY 100 (a gift from Dr. Dane Wittrup) and electroporated at 2.5 kV and 25 µF capacitance using the GenePulser (Biorad, 0.2 cm Electrode gap cuvette). The electroporated cells were grown in SD-CAA media (0.1 M sodium phosphate, pH 6.0, 6.7 g/L yeast nitrogen base, 5 g/L casamino acids, 20 g/L glucose) at 30 ^oC and 250 rpm. Frozen aliquots of the library were prepared by freezing 10x library diversity in yeast freezing media (2 % glycerol and 6.7 g/L yeast nitrogen base) at - 80 ^oC for long-term storage.

For the following rounds of gene diversification, it was realized by shuffling the library screened in the previous round, followed by the above random mutagenesis procedure to incorporate additional mutations. The plasmid DNA from the library pool was isolated using a yeast plasmid miniprep kit (Zymo Research). pT231 scFv library gene was PCR amplified with primers flanking the region. 2-4 µg of the PCR product was digested with 0.0015 unit of DNase I (New England BioLabs) per µL in 100 µL of reaction mixture for 15 min at room temperature. Fragments of 10-50 bp were purified from 2 % low melting agarose gel by electrophoresis and then re-suspended in 50 µL of PCR reaction without

primers. A PCR program of 94 °C for 3 min; 29 cycles of 94 °C for 30 s, 55 °C for 30 s, 72 °C for 30 s, and 72 °C for 10 min was used on a thermocycler. Mixtures of DNA fragments were reassembled into a gene at defined positions based on gene homology.

Fluorescence activated cell sorting was used to screen for yeast cells displaying high-affinity scFvs. 10x library diversity of cells were pelleted and washed with 1 mL of phosphate-buffered saline with bovine serum albumin (PBSA, 8 g/L NaCl, 0.2 g/L KCl, 1.44 g/L Na_2HPO_4, 0.24 g/L KH_2PO_4, 1 g/L bovine serum albumin, pH 7.4) twice. The cells were incubated with Pphos-b in 3 mL PBSA at room temperature for 1 hour. After labeling with peptide, the cells were primarily stained with mouse anti-FLAG (Sigma, 1:1000 dilution) in 1 mL of PBSA on ice for 30 min, and then secondarily stained with goat anti-mouse Alexa Fluor 488 (Thermo Fisher Scientific, 1:100 dilution) and streptavidin R-phycoerythrin (SAPE, Thermo Fisher Scientific, 1:100 dilution) in 1 mL of PBSA on ice for 30 min. Pelleting and washing the cells with 500 µL of PBSA were required between all labeling steps to remove any unbound peptides and antibodies. After labeling, the cells were re-suspended in 3 mL of PBSA and treated with 1 µM of unmodified phosphopeptide at room temperature for 7 min. The screening was carried out on a Becton-Dickinson FACSAria II, which was equipped with five different lasers. Data of cell screening was acquired using BD FACSDiva software. The collected cells were grown in SD-CAA media plus 1 % kanamycin at 30 °C, 250 rpm overnight. After several rounds of cell propagation, 10x library diversity of cells were archived in yeast freezing media at -80 °C.

Purification of pT231 scFvs

The pT231 scFv gene was inserted into the vector pRS316 (a gift from Dr. Eric Shusta), which had been restriction-digested with *Nhe*I and *BsrG*I (New England Biolabs). This plasmid included a C-terminal hexa-histidine epitope tag. The pRS316 plasmid was transformed into *S. cerevisiae* YVH10 cells (72) (a gift from Dr. Eric Shusta) for protein secretion and purification.

Cells were grown in 500 mL of SD-CAA plus tryptophan media at 30 °C, 250 rpm for 3 days, pelleted, and re-suspended in 500 mL of SG-CAA plus tryptophan with 0.1% bovine serum albumin (Sigma-Aldrich) at 20 °C, 250 rpm for 3 days to induce and secrete the scFvs. The cells were pelleted, and supernatant containing scFv was collected and filtered using bottle-top filter (Corning, PES membrane, 0.22 µm) to remove the yeast cells and cell lysate. The scFv supernatant was firstly concentrated to 50 mL by ultrafiltration using a selective permeable membrane (MilliporeSigma, 10 kDa) under nitrogen pressure. The concentrated supernatant was then dialyzed to exchange buffer in 5 L of phosphate-buffered saline (0.01 M sodium phosphate, 0.15 M NaCl, pH 8.0) at 4 °C overnight. The dialyzed scFvs solution was purified as described previously (46), using the SuperFlow Ni-NTA beads (Qiagen). The purified scFvs were resolved using SDS-PAGE in tris-glycine running buffer (14.4 g/L glycine, 1 g/L SDS, 3.03 g/L Tris base) with 12 % Bis-Tris gels. SeeBlue® pre-stained protein standard (Thermo Fisher Scientific) was used to determine the molecular weights.

Fluorescent tagging of purified pT231 scFvs

The scFv elution fractions were pooled and concentrated using a centrifugal filter unit (MilliporeSigma, Amicon Ultra, 10 kDa MWCO). The concentrated scFvs were diluted to 3 mg/mL in 0.1 M sodium bicarbonate buffer at pH 8.3. The amine-reactive dye Alexa Fluor 594 NHS ester (Thermo Fisher Scientific) was prepared in dimethylformamide (DMF) at 10 mg/mL immediately before use. 35 µg of Alexa Fluor 594 NHS ester from the stock solution was added to 100 µg of purified scFv. The reaction mixture was incubated for 1 hour at room temperature in the dark. Unreacted dye was removed using the Zeba desalting columns (Thermo Fisher Scientific, 7 kDa MWCO), and the concentrations of modified scFvs were determined using a Bradford assay (Thermo Fisher Scientific).

Immunocytochemistry in HEK 293 cells

The HEK 293 cells were transfected with pRK5-EGFP-Tau (Addgene 46904), which contained human tau (MAPT 0N4R) fused to EGFP at the N-terminus. Cells were rinsed once with 0.5 mL of ice-cold PBSCM buffer (0.15 M NaCl, 1.9 mM NaH_2PO_4, 8.1 mM Na_2HPO_4, 1 mM $CaCl_2$, 0.5 mM Mg_2SO_4, pH 7.4), fixed in 4% paraformaldehyde (Sigma) in PBSCM at room temperature for 15 min, and then permeabilized using 0.1% Triton X-100 (Acros Organics) in

PBSCM at room temperature for 15 min. After washing three times with PBSCM, the cells incubated with 0.1 μM of Alexa Fluor 594 conjugated scFv in 0.5 mL of PBSCM with 40% goat serum (PBSG) at 4 ^{o}C overnight in the dark. The cells were washed three times with ice cold 0.5 mL PBSCM, stained with 0.3 μM of DAPI (Thermo Fisher Scientific) at room temperature for 5 min, washed once with 0.5 mL of ice-cold PBSCM. The cells were imaged using a Nikon A1R confocal microscope (UConn Center for Open Research Resources and Equipment).

Immunohistochemistry in brain tissue sections

All mouse (n=3 PS19, 3 wild-type C57BL6/J, and 3 tau knock-out) and human (n=2 AD cases and n=2 aged control) tissues were sectioned at 30 μm stained as free floating sections using Netwell baskets (VWR Cat#29442-132) in 12-well Falcon plates (Cat#353043). Extracted mouse tissues were flash frozen on dry ice, sectioned onto slides (Millenia 2.0 Adhesion Slides Catalog # 318), and fixed in cold 4% PFA for 3 minutes prior to staining. Human tissues were fixed and stored in PLP until sectioned using a Leica VT1200S vibratome. To quench lipofuscin autofluorescence, human tissue sections were photobleached under a 1500 lumen white LED bulb for 72 hours at 4°C while suspended in PBS with no lid or covering (73). Following mouse tissue fixation and human tissue bleaching, all sections were then washed three times in PBS for 30 seconds per wash followed by a 5-minute incubation in detergent media (TBS with 0.25% Triton-X). Tissue was then incubated for 30 minutes in citrate-based antigen unmasking solution (Vector Cat#H-3300) at 95°C. Tissue was blocked with gentle rotating for 2 hours in detergent media with 5% donkey serum (Sigma-Aldrich D9663-10mL). After blocking, free floating human tissue sections were moved into separate wells of a 24-well plate with 300 μL of the appropriate scFv dilution and no basket; mouse tissue was stained directly on the slides with 200 μL of the appropriate scFv dilution. Tissues were incubated with the scFvs for 3 hours at room temperature with gentle rotation.

Following scFv incubation, tissue sections were incubated with 1 μg/mL of DAPI in the dark for 5 minutes at room temperature. Tissues were then washed four times in PBS for 5 minutes each and carefully placed on Millenia 2.0 slides using a histology brush if free floating (Fisher Scientific Cat#NC0344756). Excess water was allowed to evaporate for 15 minutes, then each slide was mounted with 100uL of Prolong Gold Antifade Reagent (Thermo Fisher Cat#P36930) and a 1 mm cover slip. Imaging was done using a Zeiss LSM 710 confocal microscope, ensuring equal parameters for digital gain (790), pinhole (30 um), and laser power (4.4%) for all images. Following imaging, images were processed using the Fiji distribution of ImageJ. The magic wand tool was used to select individual tangles as a region of interest (ROI) which was then measured for average fluorescence intensity.

Acknowledgments

We thank You-Jun Fu for assistance with mass spectrometry of purified peptides. Human brain tissue was generously provided by the National Institute of Aging Boston University AD Center (P30AG13846). We would like to thank the following funding agencies for their support: YKC: NIH (NS099903), NSF (1706743), Brain and Behavior Research Foundation (NARSAD Young Investigator); BW: NIH (AG050471, NS089544, ES020395), BrightFocus Foundation, Alzheimer Association, Cure Alzheimer's Fund and the Edward N. and Della L. Thome Memorial Foundation; BM: NS106751. The content is solely the responsibility of the authors and does not necessarily represent the official views of the National Institutes of Health.

Conflict of interest

BW is co-founder and chief scientific officer of Aquinnah Pharmaceuticals Inc. All other authors declare that they have no conflicts of interest with the contents of this article.

References

1. Rush, J., Moritz, A., Lee, K. A., Guo, A., Goss, V. L., Spek, E. J., Zhang, H., Zha, X. M., Polakiewicz, R. D., and Comb, M. J. (2005) Immunoaffinity profiling of tyrosine phosphorylation in cancer cells. *Nat Biotechnol* 23, 94-101
2. van der Mijn, J. C., Labots, M., Piersma, S. R., Pham, T. V., Knol, J. C., Broxterman, H. J., Verheul, H. M., and Jimenez, C. R. (2015) Evaluation of different phospho-tyrosine antibodies for label-free phosphoproteomics. *J Proteomics* 127, 259-263
3. Khoury, G. A., Baliban, R. C., and Floudas, C. A. (2011) Proteome-wide post-translational modification statistics: frequency analysis and curation of the swiss-prot database. *Sci Rep* 1
4. Li, C., and Gotz, J. (2017) Tau-based therapies in neurodegeneration: opportunities and challenges. *Nature Reviews. Drug Discovery* 16, 863-883
5. Guo, T., Noble, W., and Hanger, D. P. (2017) Roles of tau protein in health and disease. *Acta Neuropathol* 133, 665-704
6. Morris, M., Knudsen, G. M., Maeda, S., Trinidad, J. C., Ioanoviciu, A., Burlingame, A. L., and Mucke, L. (2015) Tau post-translational modifications in wild-type and human amyloid precursor protein transgenic mice. *Nat Neurosci* 18, 1183-1189
7. Kopke, E., Tung, Y. C., Shaikh, S., Alonso, A. C., Iqbal, K., and Grundke-Iqbal, I. (1993) Microtubule-associated protein tau. Abnormal phosphorylation of a non-paired helical filament pool in Alzheimer disease. *J Biol Chem* 268, 24374-24384
8. Drewes, G., Trinczek, B., Illenberger, S., Biernat, J., Schmitt-Ulms, G., Meyer, H. E., Mandelkow, E. M., and Mandelkow, E. (1995) Microtubule-associated protein/microtubule affinity-regulating kinase (p110mark). A novel protein kinase that regulates tau-microtubule interactions and dynamic instability by phosphorylation at the Alzheimer-specific site serine 262. *J Biol Chem* 270, 7679-7688
9. Sengupta, A., Kabat, J., Novak, M., Wu, Q., Grundke-Iqbal, I., and Iqbal, K. (1998) Phosphorylation of tau at both Thr 231 and Ser 262 is required for maximal inhibition of its binding to microtubules. *Arch Biochem Biophys* 357, 299-309
10. von Bergen, M., Friedhoff, P., Biernat, J., Heberle, J., Mandelkow, E. M., and Mandelkow, E. (2000) Assembly of tau protein into Alzheimer paired helical filaments depends on a local sequence motif ((306)VQIVYK(311)) forming beta structure. *Proc Natl Acad Sci U S A* 97, 5129-5134
11. Berger, Z., Roder, H., Hanna, A., Carlson, A., Rangachari, V., Yue, M., Wszolek, Z., Ashe, K., Knight, J., Dickson, D., Andorfer, C., Rosenberry, T. L., Lewis, J., Hutton, M., and Janus, C. (2007) Accumulation of pathological tau species and memory loss in a conditional model of tauopathy. *J Neurosci* 27, 3650-3662
12. Min, S. W., Cho, S. H., Zhou, Y., Schroeder, S., Haroutunian, V., Seeley, W. W., Huang, E. J., Shen, Y., Masliah, E., Mukherjee, C., Meyers, D., Cole, P. A., Ott, M., and Gan, L. (2010) Acetylation of tau inhibits its degradation and contributes to tauopathy. *Neuron* 67, 953-966
13. Cohen, T. J., Guo, J. L., Hurtado, D. E., Kwong, L. K., Mills, I. P., Trojanowski, J. Q., and Lee, V. M. (2011) The acetylation of tau inhibits its function and promotes pathological tau aggregation. *Nat Commun* 2, 252
14. Irwin, D. J., Cohen, T. J., Grossman, M., Arnold, S. E., McCarty-Wood, E., Van Deerlin, V. M., Lee, V. M., and Trojanowski, J. Q. (2013) Acetylated tau neuropathology in sporadic and hereditary tauopathies. *Am J Pathol* 183, 344-351
15. Min, S. W., Chen, X., Tracy, T. E., Li, Y., Zhou, Y., Wang, C., Shirakawa, K., Minami, S. S., Defensor, E., Mok, S. A., Sohn, P. D., Schilling, B., Cong, X., Ellerby, L., Gibson, B. W., Johnson, J., Krogan, N., Shamloo, M., Gestwicki, J., Masliah, E., Verdin, E., and Gan, L. (2015) Critical role of acetylation in tau-mediated neurodegeneration and cognitive deficits. *Nat Med* 10.1038/nm.3951
16. Bayes, A., and Grant, S. G. (2009) Neuroproteomics: understanding the molecular organization and complexity of the brain. *Nat Rev Neurosci* 10, 635-646
17. Prabakaran, S., Lippens, G., Steen, H., and Gunawardena, J. (2012) Post-translational modification: nature's escape from genetic imprisonment and the basis for dynamic information encoding. *Wiley Interdiscip Rev Syst Biol Med* 4, 565-583
18. Witze, E. S., Old, W. M., Resing, K. A., and Ahn, N. G. (2007) Mapping protein post-translational modifications with mass spectrometry. *Nat Methods* 4, 798-806
19. Lothrop, A. P., Torres, M. P., and Fuchs, S. M. (2013) Deciphering post-translational modification codes. *FEBS Lett* 587, 1247-1257
20. Rosseels, J., Van den Brande, J., Violet, M., Jacobs, D., Grognet, P., Lopez, J., Huvent, I., Caldara, M., Swinnen, E., Papegaey, A., Caillierez, R., Buee-Scherrer, V., Engelborghs, S., Lippens, G., Colin, M.,

Buee, L., Galas, M. C., Vanmechelen, E., and Winderickx, J. (2015) Tau monoclonal antibody generation based on humanized yeast models: impact on Tau oligomerization and diagnostics. *J Biol Chem* 290, 4059-4074

21. d'Abramo, C., Acker, C. M., Jimenez, H. T., and Davies, P. (2013) Tau passive immunotherapy in mutant P301L mice: antibody affinity versus specificity. *PLoS One* 8, e62402
22. Brumbaugh, K., Johnson, W., Liao, W. C., Lin, M. S., Houchins, J. P., Cooper, J., Stoesz, S., and Campos-Gonzalez, R. (2011) Overview of the generation, validation, and application of phosphosite-specific antibodies. *Methods Mol Biol* 717, 3-43
23. Czernik, A. J., Girault, J. A., Nairn, A. C., Chen, J., Snyder, G., Kebabian, J., and Greengard, P. (1991) Production of phosphorylation state-specific antibodies. *Methods Enzymol* 201, 264-283
24. Batista, F. D., and Neuberger, M. S. (1998) Affinity dependence of the B cell response to antigen: a threshold, a ceiling, and the importance of off-rate. *Immunity* 8, 751-759
25. Foote, J., and Eisen, H. N. (1995) Kinetic and affinity limits on antibodies produced during immune responses. *Proc Natl Acad Sci U S A* 92, 1254-1256
26. Koerber, J. T., Thomsen, N. D., Hannigan, B. T., Degrado, W. F., and Wells, J. A. (2013) Nature-inspired design of motif-specific antibody scaffolds. *Nat Biotechnol* 31, 916-921
27. Shih, H. H., Tu, C., Cao, W., Klein, A., Ramsey, R., Fennell, B. J., Lambert, M., Ni Shuilleabhain, D., Autin, B., Kouranova, E., Laxmanan, S., Braithwaite, S., Wu, L., Ait-Zahra, M., Milici, A. J., Dumin, J. A., LaVallie, E. R., Arai, M., Corcoran, C., Paulsen, J. E., Gill, D., Cunningham, O., Bard, J., Mosyak, L., and Finlay, W. J. (2012) An ultra-specific avian antibody to phosphorylated tau protein reveals a unique mechanism for phosphoepitope recognition. *J Biol Chem* 287, 44425-44434
28. Feldhaus, M. J., Siegel, R. W., Opresko, L. K., Coleman, J. R., Feldhaus, J. M., Yeung, Y. A., Cochran, J. R., Heinzelman, P., Colby, D., Swers, J., Graff, C., Wiley, H. S., and Wittrup, K. D. (2003) Flow-cytometric isolation of human antibodies from a nonimmune Saccharomyces cerevisiae surface display library. *Nat Biotechnol* 21, 163-170
29. Kehoe, J. W., Velappan, N., Walbolt, M., Rasmussen, J., King, D., Lou, J., Knopp, K., Pavlik, P., Marks, J. D., Bertozzi, C. R., and Bradbury, A. R. (2006) Using phage display to select antibodies recognizing post-translational modifications independently of sequence context. *Mol Cell Proteomics* 5, 2350-2363
30. Fuchs, S. M., Krajewski, K., Baker, R. W., Miller, V. L., and Strahl, B. D. (2011) Influence of combinatorial histone modifications on antibody and effector protein recognition. *Curr Biol* 21, 53-58
31. Bock, I., Dhayalan, A., Kudithipudi, S., Brandt, O., Rathert, P., and Jeltsch, A. (2011) Detailed specificity analysis of antibodies binding to modified histone tails with peptide arrays. *Epigenetics* 6, 256-263
32. Egelhofer, T. A., Minoda, A., Klugman, S., Lee, K., Kolasinska-Zwierz, P., Alekseyenko, A. A., Cheung, M. S., Day, D. S., Gadel, S., Gorchakov, A. A., Gu, T., Kharchenko, P. V., Kuan, S., Latorre, I., Linder-Basso, D., Luu, Y., Ngo, Q., Perry, M., Rechtsteiner, A., Riddle, N. C., Schwartz, Y. B., Shanower, G. A., Vielle, A., Ahringer, J., Elgin, S. C., Kuroda, M. I., Pirrotta, V., Ren, B., Strome, S., Park, P. J., Karpen, G. H., Hawkins, R. D., and Lieb, J. D. (2011) An assessment of histone-modification antibody quality. *Nat Struct Mol Biol* 18, 91-93
33. Petry, F. R., Pelletier, J., Bretteville, A., Morin, F., Calon, F., Hebert, S. S., Whittington, R. A., and Planel, E. (2014) Specificity of anti-tau antibodies when analyzing mice models of Alzheimer's disease: problems and solutions. *PLoS One* 9, e94251
34. Ercan, E., Eid, S., Weber, C., Kowalski, A., Bichmann, M., Behrendt, A., Matthes, F., Krauss, S., Reinhardt, P., Fulle, S., and Ehrnhoefer, D. E. (2017) A validated antibody panel for the characterization of tau post-translational modifications. *Mol Neurodegener* 12, 87
35. Boder, E. T., and Wittrup, K. D. (1997) Yeast surface display for screening combinatorial polypeptide libraries. *Nat Biotechnol* 15, 553-557
36. Cho, Y. K., Chen, I., Wei, X., Li, L., and Shusta, E. V. (2009) A yeast display immunoprecipitation method for efficient isolation and characterization of antigens. *J Immunol Methods* 341, 117-126
37. Krishnaswamy, S., Lin, Y., Rajamohamedsait, W. J., Rajamohamedsait, H. B., Krishnamurthy, P., and Sigurdsson, E. M. (2014) Antibody-derived in vivo imaging of tau pathology. *J Neurosci* 34, 16835-16850
38. Nisbet, R. M., Van der Jeugd, A., Leinenga, G., Evans, H. T., Janowicz, P. W., and Gotz, J. (2017) Combined effects of scanning ultrasound and a tau-specific single chain antibody in a tau transgenic mouse model. *Brain* 140, 1220-1230
39. Ising, C., Gallardo, G., Leyns, C. E. G., Wong, C. H., Stewart, F., Koscal, L. J., Roh, J., Robinson, G. O., Remolina Serrano, J., and Holtzman, D. M. (2017) AAV-mediated expression of anti-tau scFvs decreases tau accumulation in a mouse model of tauopathy. *J Exp Med* 214, 1227-1238

40. Liu, H. L., Hsu, P. H., Lin, C. Y., Huang, C. W., Chai, W. Y., Chu, P. C., Huang, C. Y., Chen, P. Y., Yang, L. Y., Kuo, J. S., and Wei, K. C. (2016) Focused Ultrasound Enhances Central Nervous System Delivery of Bevacizumab for Malignant Glioma Treatment. *Radiology* 281, 99-108
41. Razai, A., Garcia-Rodriguez, C., Lou, J., Geren, I. N., Forsyth, C. M., Robles, Y., Tsai, R., Smith, T. J., Smith, L. A., Siegel, R. W., Feldhaus, M., and Marks, J. D. (2005) Molecular evolution of antibody affinity for sensitive detection of botulinum neurotoxin type A. *J Mol Biol* 351, 158-169
42. Oi, V. T., Glazer, A. N., and Stryer, L. (1982) Fluorescent phycobiliprotein conjugates for analyses of cells and molecules. *J Cell Biol* 93, 981-986
43. Zaccolo, M., Williams, D. M., Brown, D. M., and Gherardi, E. (1996) An approach to random mutagenesis of DNA using mixtures of triphosphate derivatives of nucleoside analogues. *J Mol Biol* 255, 589-603
44. Swers, J. S., Kellogg, B. A., and Wittrup, K. D. (2004) Shuffled antibody libraries created by in vivo homologous recombination and yeast surface display. *Nucleic Acids Res* 32, e36
45. Boder, E. T., and Wittrup, K. D. (1998) Optimal screening of surface-displayed polypeptide libraries. *Biotechnol Prog* 14, 55-62
46. Huang, D., and Shusta, E. V. (2005) Secretion and surface display of green fluorescent protein using the yeast Saccharomyces cerevisiae. *Biotechnol Prog* 21, 349-357
47. Hackel, B. J., Huang, D., Bubolz, J. C., Wang, X. X., and Shusta, E. V. (2006) Production of soluble and active transferrin receptor-targeting single-chain antibody using Saccharomyces cerevisiae. *Pharm Res* 23, 790-797
48. Hoover, B. R., Reed, M. N., Su, J., Penrod, R. D., Kotilinek, L. A., Grant, M. K., Pitstick, R., Carlson, G. A., Lanier, L. M., Yuan, L. L., Ashe, K. H., and Liao, D. (2010) Tau mislocalization to dendritic spines mediates synaptic dysfunction independently of neurodegeneration. *Neuron* 68, 1067-1081
49. Tak, H., Haque, M. M., Kim, M. J., Lee, J. H., Baik, J. H., Kim, Y., Kim, D. J., Grailhe, R., and Kim, Y. K. (2013) Bimolecular fluorescence complementation; lighting-up tau-tau interaction in living cells. *PLoS One* 8, e81682
50. Coutadeur, S., Benyamine, H., Delalonde, L., de Oliveira, C., Leblond, B., Foucourt, A., Besson, T., Casagrande, A. S., Taverne, T., Girard, A., Pando, M. P., and Desire, L. (2015) A novel DYRK1A (dual specificity tyrosine phosphorylation-regulated kinase 1A) inhibitor for the treatment of Alzheimer's disease: effect on Tau and amyloid pathologies in vitro. *J Neurochem* 133, 440-451
51. Yoshiyama, Y., Higuchi, M., Zhang, B., Huang, S. M., Iwata, N., Saido, T. C., Maeda, J., Suhara, T., Trojanowski, J. Q., and Lee, V. M. (2007) Synapse loss and microglial activation precede tangles in a P301S tauopathy mouse model. *Neuron* 53, 337-351
52. Boder, E. T., Midelfort, K. S., and Wittrup, K. D. (2000) Directed evolution of antibody fragments with monovalent femtomolar antigen-binding affinity. *Proc Natl Acad Sci U S A* 97, 10701-10705
53. Foote, J., and Winter, G. (1992) Antibody framework residues affecting the conformation of the hypervariable loops. *J Mol Biol* 224, 487-499
54. Wedemayer, G. J., Patten, P. A., Wang, L. H., Schultz, P. G., and Stevens, R. C. (1997) Structural insights into the evolution of an antibody combining site. *Science* 276, 1665-1669
55. Furukawa, K., Akasako-Furukawa, A., Shirai, H., Nakamura, H., and Azuma, T. (1999) Junctional amino acids determine the maturation pathway of an antibody. *Immunity* 11, 329-338
56. Manivel, V., Sahoo, N. C., Salunke, D. M., and Rao, K. V. (2000) Maturation of an antibody response is governed by modulations in flexibility of the antigen-combining site. *Immunity* 13, 611-620
57. Yin, J., Beuscher, A. E. t., Andryski, S. E., Stevens, R. C., and Schultz, P. G. (2003) Structural plasticity and the evolution of antibody affinity and specificity. *J Mol Biol* 330, 651-656
58. Adhikary, R., Yu, W., Oda, M., Walker, R. C., Chen, T., Stanfield, R. L., Wilson, I. A., Zimmermann, J., and Romesberg, F. E. (2015) Adaptive mutations alter antibody structure and dynamics during affinity maturation. *Biochemistry* 54, 2085-2093
59. Baybutt, H., and Manson, J. (1997) Characterisation of two promoters for prion protein (PrP) gene expression in neuronal cells. *Gene* 184, 125-131
60. Hoffmann, N. A., Dorostkar, M. M., Blumenstock, S., Goedert, M., and Herms, J. (2013) Impaired plasticity of cortical dendritic spines in P301S tau transgenic mice. *Acta Neuropathol Commun* 1, 82
61. Schnell, U., Dijk, F., Sjollema, K. A., and Giepmans, B. N. (2012) Immunolabeling artifacts and the need for live-cell imaging. *Nat Methods* 9, 152-158
62. Helma, J., Cardoso, M. C., Muyldermans, S., and Leonhardt, H. (2015) Nanobodies and recombinant binders in cell biology. *J Cell Biol* 209, 633-644

63. Cho, J. H., and Johnson, G. V. (2004) Primed phosphorylation of tau at Thr231 by glycogen synthase kinase 3beta (GSK3beta) plays a critical role in regulating tau's ability to bind and stabilize microtubules. *J Neurochem* 88, 349-358
64. Amniai, L., Barbier, P., Sillen, A., Wieruszeski, J. M., Peyrot, V., Lippens, G., and Landrieu, I. (2009) Alzheimer disease specific phosphoepitopes of Tau interfere with assembly of tubulin but not binding to microtubules. *FASEB J* 23, 1146-1152
65. Jicha, G. A., Lane, E., Vincent, I., Otvos, L., Jr., Hoffmann, R., and Davies, P. (1997) A conformation- and phosphorylation-dependent antibody recognizing the paired helical filaments of Alzheimer's disease. *J Neurochem* 69, 2087-2095
66. Arai, H., Ishiguro, K., Ohno, H., Moriyama, M., Itoh, N., Okamura, N., Matsui, T., Morikawa, Y., Horikawa, E., Kohno, H., Sasaki, H., and Imahori, K. (2000) CSF phosphorylated tau protein and mild cognitive impairment: a prospective study. *Exp Neurol* 166, 201-203
67. Hampel, H., Burger, K., Pruessner, J. C., Zinkowski, R., DeBernardis, J., Kerkman, D., Leinsinger, G., Evans, A. C., Davies, P., Moller, H. J., and Teipel, S. J. (2005) Correlation of cerebrospinal fluid levels of tau protein phosphorylated at threonine 231 with rates of hippocampal atrophy in Alzheimer disease. *Arch Neurol* 62, 770-773
68. Kohnken, R., Buerger, K., Zinkowski, R., Miller, C., Kerkman, D., DeBernardis, J., Shen, J., Moller, H. J., Davies, P., and Hampel, H. (2000) Detection of tau phosphorylated at threonine 231 in cerebrospinal fluid of Alzheimer's disease patients. *Neurosci Lett* 287, 187-190
69. Kurosawa, N., Wakata, Y., Inobe, T., Kitamura, H., Yoshioka, M., Matsuzawa, S., Kishi, Y., and Isobe, M. (2016) Novel method for the high-throughput production of phosphorylation site-specific monoclonal antibodies. *Sci Rep* 6, 25174
70. Uhlen, M., Bandrowski, A., Carr, S., Edwards, A., Ellenberg, J., Lundberg, E., Rimm, D. L., Rodriguez, H., Hiltke, T., Snyder, M., and Yamamoto, T. (2016) A proposal for validation of antibodies. *Nat Methods* 13, 823-827
71. Burns, M. L., Malott, T. M., Metcalf, K. J., Hackel, B. J., Chan, J. R., and Shusta, E. V. (2014) Directed evolution of brain-derived neurotrophic factor for improved folding and expression in Saccharomyces cerevisiae. *Appl Environ Microbiol* 80, 5732-5742
72. Shusta, E. V., Raines, R. T., Pluckthun, A., and Wittrup, K. D. (1998) Increasing the secretory capacity of Saccharomyces cerevisiae for production of single-chain antibody fragments. *Nat Biotechnol* 16, 773-777
73. Sun, Y., Ip, P., and Chakrabartty, A. (2017) Simple Elimination of Background Fluorescence in Formalin-Fixed Human Brain Tissue for Immunofluorescence Microscopy. *J Vis Exp* 10.3791/56188

Figure 1.

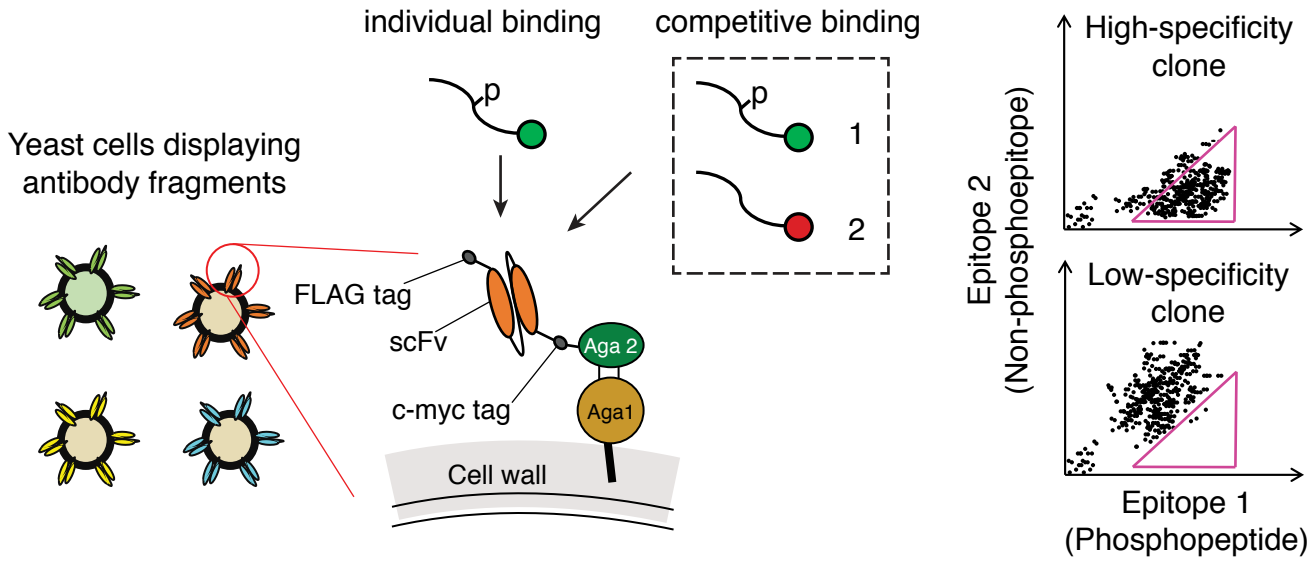

Figure 1. Schematic representation of antibody specificity quantification using yeast surface display. Individual peptide epitope binding to single chain variable region fragments displayed on yeast can be quantified. By labeling multiple peptides with distinct tags, competitive binding of potentially cross-reacting epitopes, such as a phosphopeptide and non-phosphopeptide (peptide mix indicated by a dotted box) can be quantified using multicolor flow cytometry.

Figure 2.

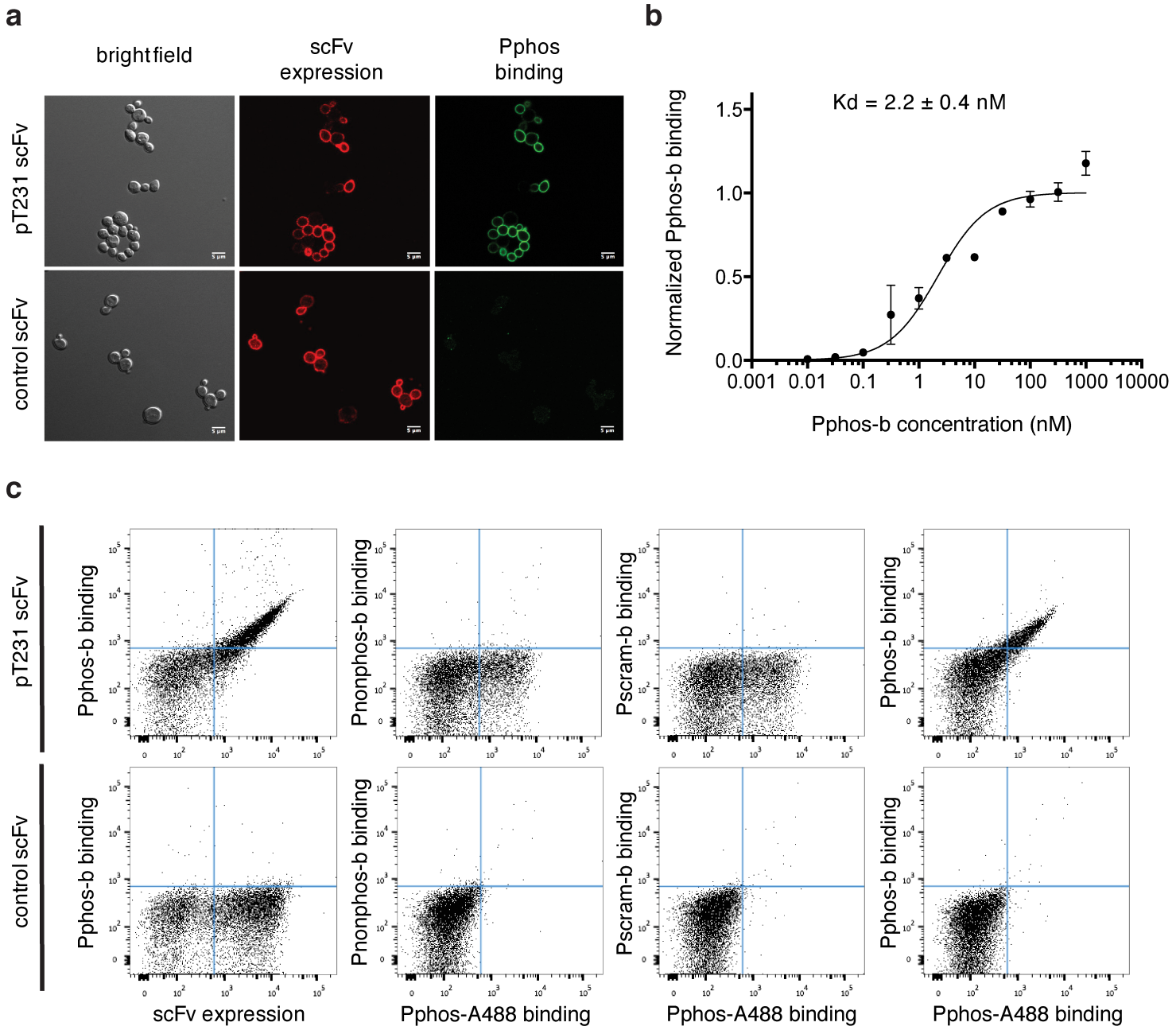

Figure 2. Characterization of yeast displayed wild-type (WT) pT231 scFv. (a) Confocal microscope images of yeast displayed wild-type pT231 scFv and an isotype-matched control scFv. scFv expression shown in red was detected using a mouse anti-FLAG antibody to assess full-length scFv expression. Cognate phosphopeptide (Pphos) binding is indicated in green. Scale bars, 5 µm. (b) Affinity measurement of yeast displayed WT pT231 scFv. The yeast cells were incubated with serial dilution of Pphos. Error bars indicate standard deviation from three independent experiments. (c) Assessment of WT pT231 scFv specificity. Flow cytometry dot plots for yeast displayed WT pT231 scFv (top row) or an isotype-matched control scFv (bottom row). The first column shows data for scFv expression and biotinylated phosphopeptide (Pphos-b) binding. In the following columns, yeast cells were incubated with a mixture of either Pnonphos-b and Pphos-A488 (second column), or Pscram-b and Pphos-A488, or Pphos-b and Pphos-A488, all at 0.5 µM.

Figure 3.

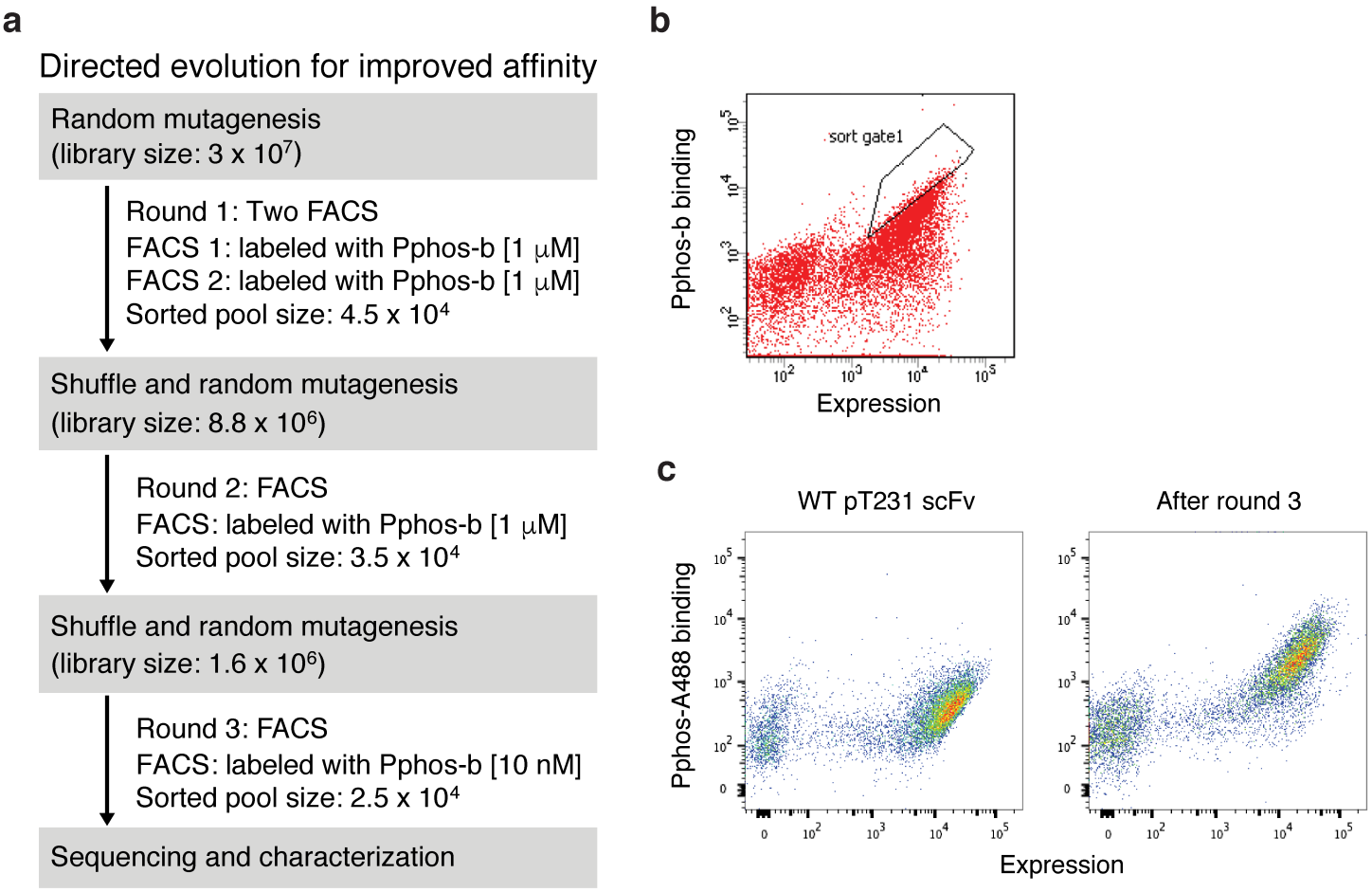

Figure 3. Directed evolution of yeast displayed pT231 scFv variants with improved affinity. (a) Flow chart for the directed evolution process. High-affinity variants were sorted using fluorescence activated cell sorting (FACS). (b) Flow cytometry dot plot with a sorting gate used for screening cells with scFv expression and high Pphos-b binding. (c) Dot plots comparing yeast displaying WT pT231 scFv (left) and a yeast pool resulting from three rounds of sorting and mutagenesis (right) were labeled for scFv expression and Pphos-A488 binding.

Figure 4.

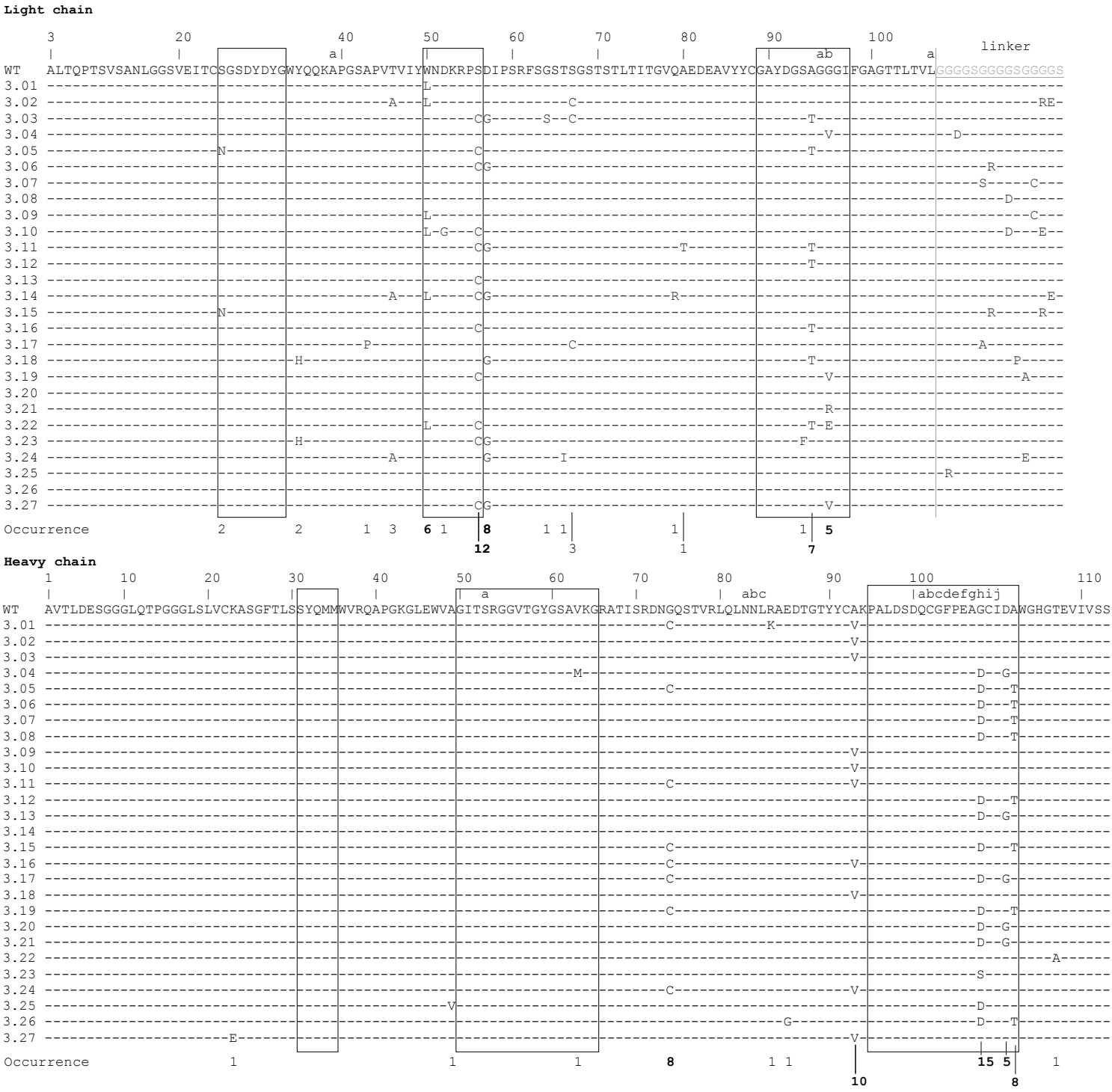

Figure 4. Amino acid sequence of individual mutants isolated from the screen for improved affinity. The sequences in the boxes indicate complementarity determining regions (CDRs). High occurrence mutations are indicated in bold. Kabat numbering is indicated at the top.

Figure 5.

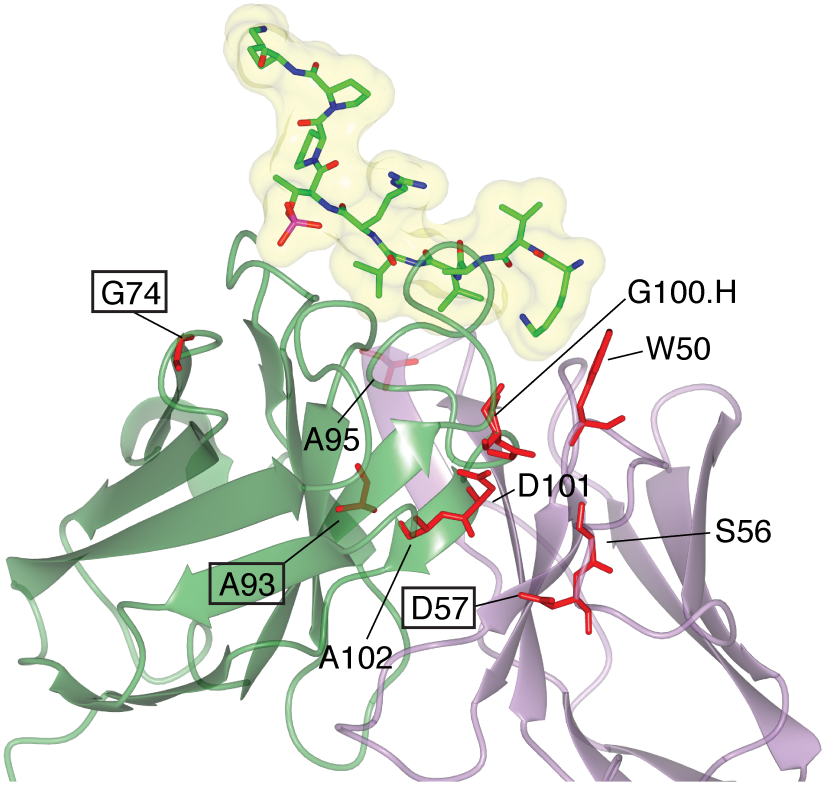

Figure 5. High occurrence mutations identified from the screen mapped on the wild-type pT231 structure. Heavy chain is shown in green and light chain in purple. Position of high occurrence mutations are indicated in red, and labeled with the wild-type amino acid. Boxed amino acids indicate those mutated in the scFv 3.24. The structure was generated using CCP4MG, based on protein data bank (PDB) entry 4GLR.

Figure 6.

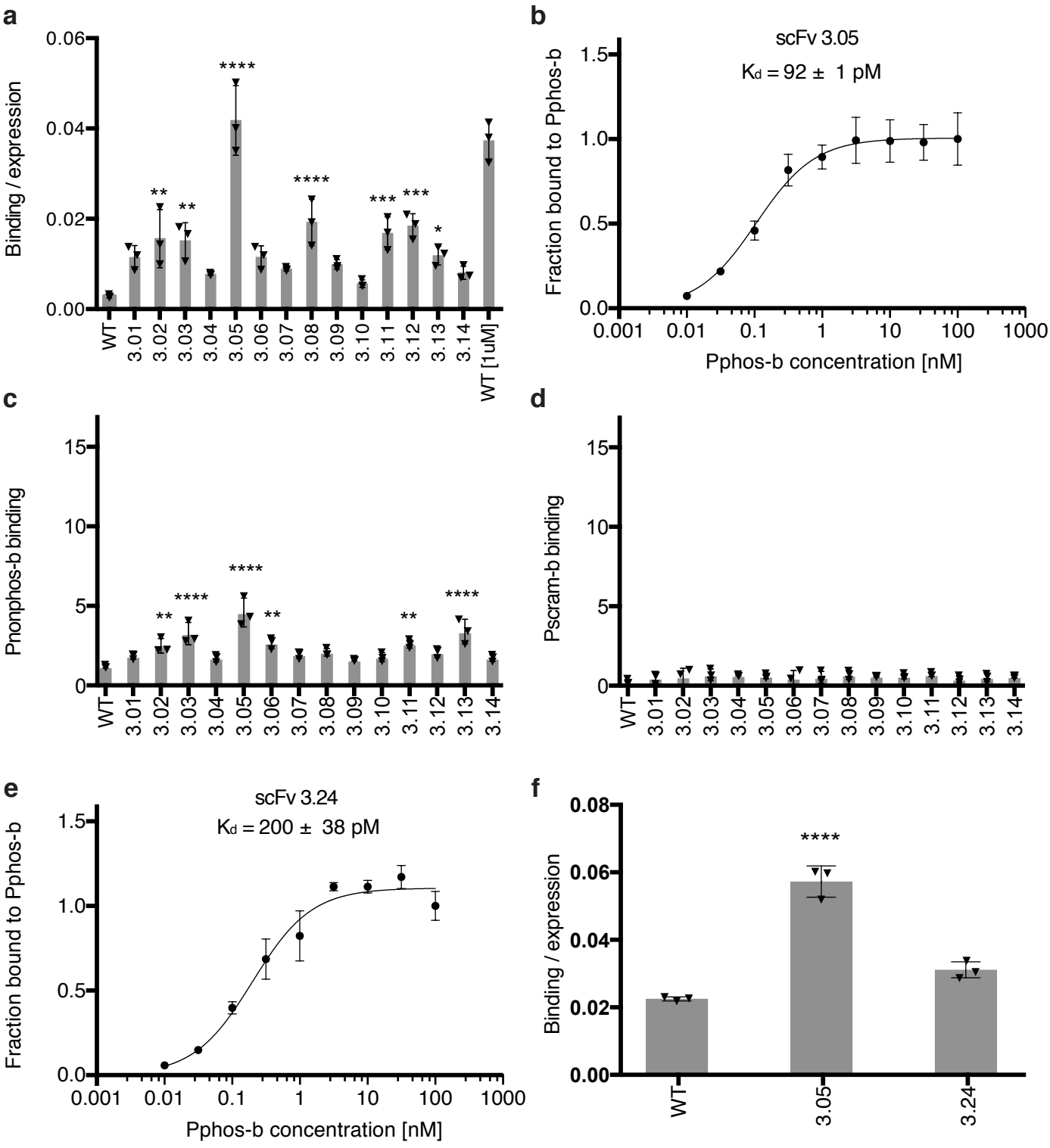

Figure 6. Characterization of affinity and specificity of individual scFvs. (a) Binding intensity normalized to the expression level of yeast displayed wild-type pT231 scFv and mutants to Pphos-b at 2 nM. The right most sample was the wild-type pT231 scFv incubated with Pphos-b at 1 μM, as a positive control. (b) Affinity titration for yeast-displayed scFv 3.05. Binding intensity of yeast displayed wild-type pT231 scFv and mutants to Pnonphos-b at 1 μM (c), and Pscram-b at 1 μM (d), respectively. (e) Affinity titration for yeast-displayed scFv 3.24. (f) Binding intensity normalized to the expression level of yeast displayed wild-type pT231 scFv and mutants to Pnonphos-b at 1 μM. Error bars indicate standard deviation from three independent experiments. Statistics for panels (a, c, d, and f): Dunnett's multiple comparisons test, $*P \leq 0.05$, $**P \leq 0.01$, $***P \leq 0.001$, $****P \leq 0.0001$, otherwise, $P > 0.05$.

Figure 7.

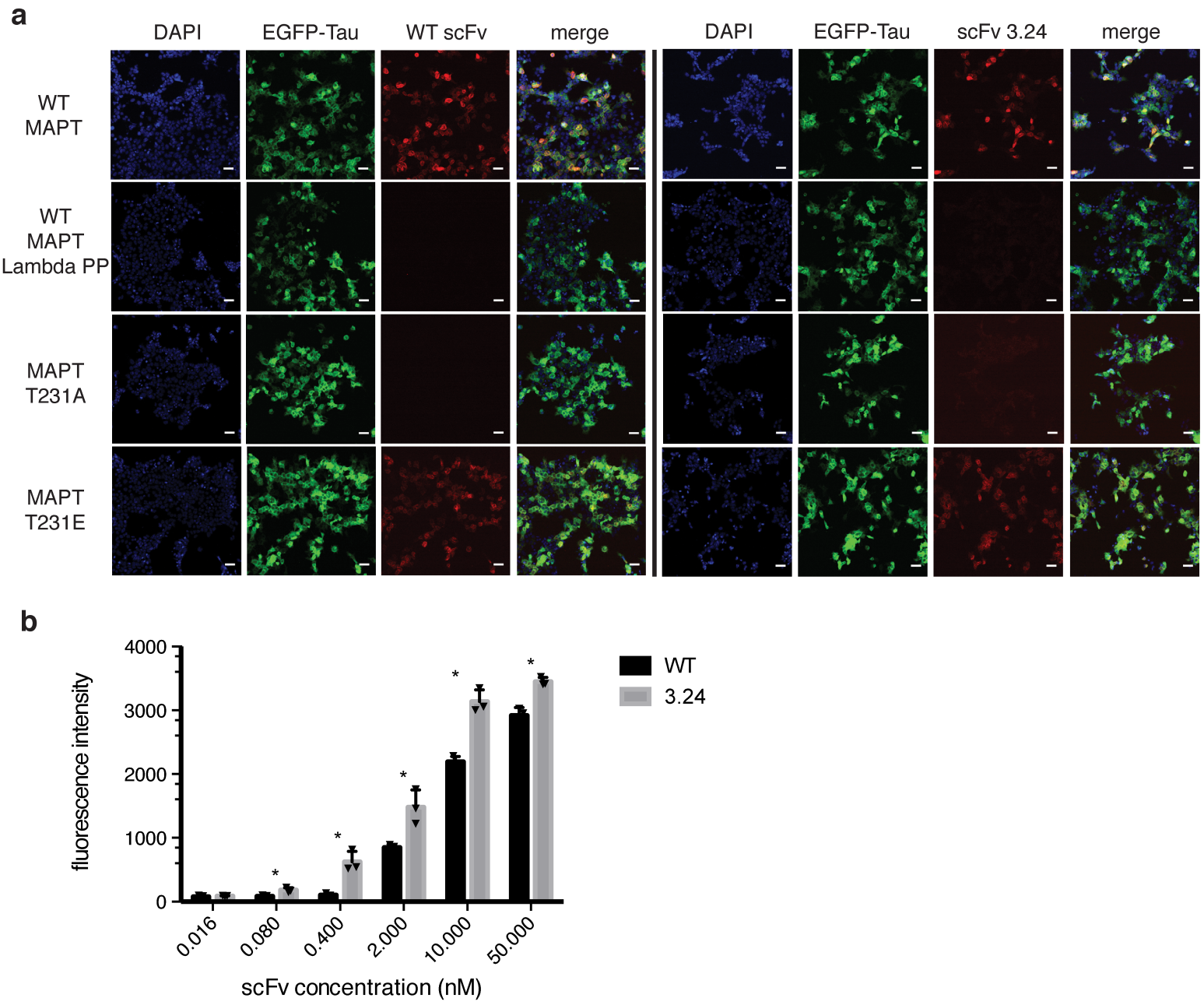

Figure 7. Cell labeling using purified pT231 scFvs. (a) Confocal microscope images of purified, fluorescently labeled WT pT231 scFv and mutant 3.24 binding to HEK293FT cells expressing wild-type tau (top row), wild-type tau treated with lambda phosphatase (second row), tau T231A (third row), and tau T231E (bottom row). All human tau constructs were fused to EGFP at the N-terminus (EGFP-tau). The first column shows DAPI staining in blue. The second column shows tau expression in green. The third column shows scFv binding in red. Scale bars, 50 µm. (b) Quantification of the fluorescence intensity of WT pT231 scFv and mutant 3.24 binding to HEK293FT cells expressing wild-type tau at scFv concentrations from 16 pM to 50 nM. Error bars indicate standard deviation from three independent experiments. Statistics for panel (b): Student's t-test, $*P \leq 0.05$.

Figure 8.

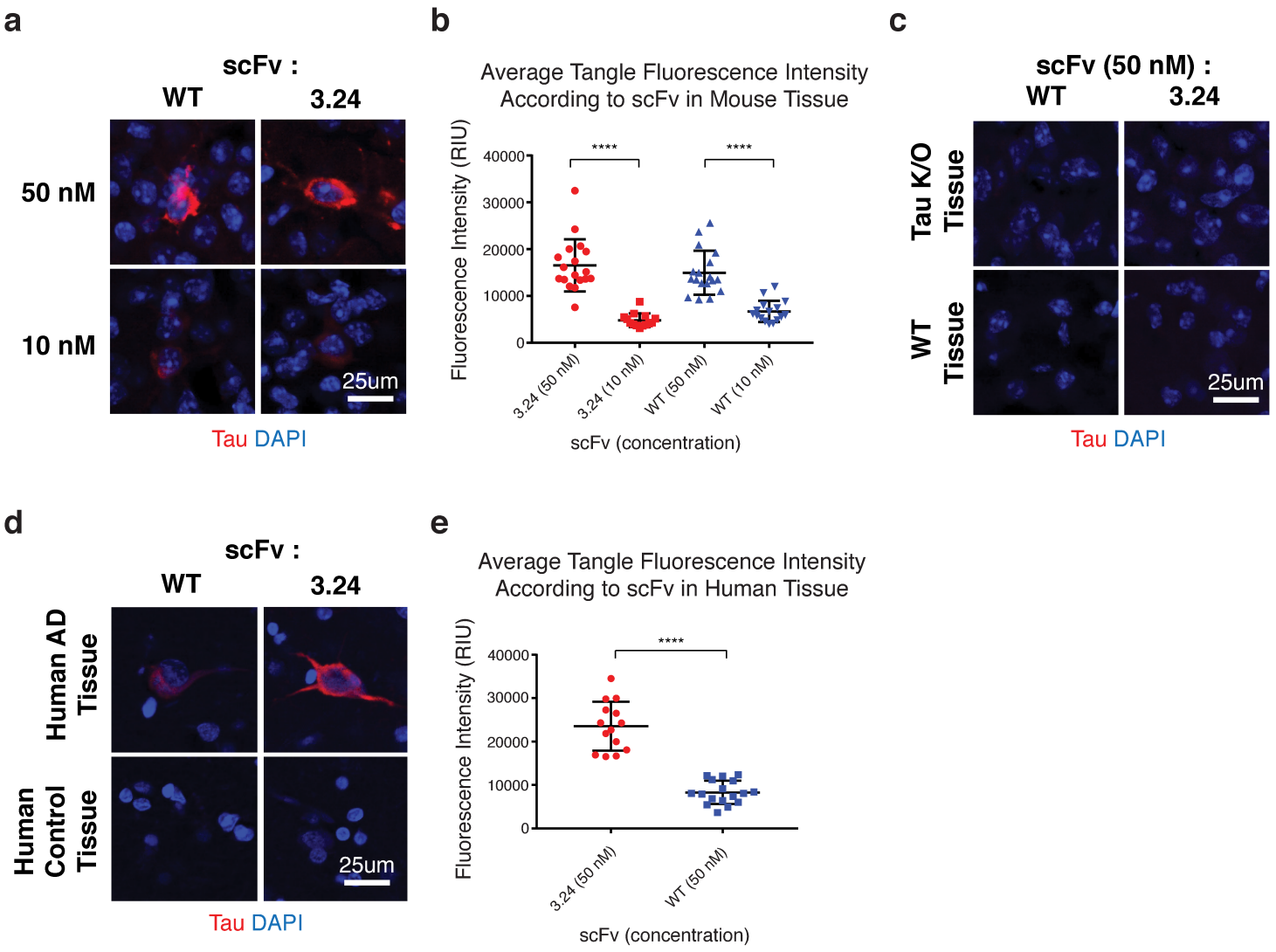

Figure 8. Tissue labeling using purified pT231 scFvs. (a) Immunohistochemistry using the scFvs on brain slices of 8-month old mice expressing P301S mutant tau indicates that both scFvs robustly identify neurofibrillary tangles in tissue. Each scFv was used at 50 nM and 10 nM to identify optimal staining concentrations and show a dose response for staining intensity, quantified in (b). Tau is shown in red with nuclei stained using DAPI in blue. The 10nM concentrations showed significant reduction in staining intensity for both the WT and 3.24 scFv ($P < 0.0001$ by one-way ANOVA with $P < 0.0001$ between the 50 nM and 10 nM working concentrations of each scFv using Tukey's multiple comparisons test). There were no statistical differences between the WT and 3.24 scFv at either concentration. (c) Neither scFv stained wild-type or tau knockout mouse tissue at the 50 nM working concentration, indicating no off target staining or background fluorescence. (d) Immunohistochemistry of human AD and aged control tissues also indicate that both scFvs stain phospho-tau tangles in disease (scFv concentration = 50 nM). However, in the human tissue the high affinity scFv 3.24 shows a significant increase in staining intensity compared to the WT scFv, which is quantified in (e) ($P < 0.0001$ using a two-sample t-test assuming unequal variances).

Directed Evolution of a Picomolar Affinity High Specificity Antibody Targeting Phosphorylated Tau

Dan Li, Lei Wang, Brandon F. Maziuk, Xudong Yao, Benjamin Wolozin and Yong Ku Cho

J. Biol. Chem. published online June 13, 2018
